

Sedimentation equilibrium and gravity dependent stiffness coefficients of colloidal hard-spheres

Luis G. MacDowell¹ and Eva G. Noya²

¹*Departamento de Química Física (Unidad Asociada de I+D+i al CSIC), Facultad de Ciencias Químicas, Universidad Complutense de Madrid, Madrid, 28040, Spain.* ^{a)}

²*Instituto de Química Física Blas Cabrera, CSIC, Calle Serrano 119, 28006 Madrid, Spain.* ^{b)}

(Dated: 9 July 2026)

Spherical colloids with harsh repulsive forces have long been used as experimental analogs of the hard sphere model, with demonstrated good agreement with computer simulations for bulk and structural properties of the fluid, glass and crystal phases. However, an enigmatic discrepancy remains for the crystal-melt stiffness coefficient. Here we perform computer simulations of colloidal hard spheres under tunable buoyant mass and show that the long-standing discrepancy can be traced to a hitherto unrecognized gravity dependent contribution of the stiffness coefficient. This effect is one practical realization of a more general result for the external field dependence of stiffness coefficients of arbitrary interfaces.

PACS numbers: Valid PACS appear here

Keywords: Suggested keywords

I. INTRODUCTION

Hard spheres remain to date one of the cornerstones of statistical mechanics, and have helped us shape our understanding of entropy driven phenomena in soft matter physics.¹ The confirmation of a freezing transition in hard spheres was likely the first milestone of molecular simulations,^{2,3} and played a fundamental role in appreciating the significance of harsh repulsive forces.⁴ The significance of this one step beyond the ideal gas system has ever since become enormous. In statistical thermodynamics it is the fundamental ingredient of perturbation theories of the liquid state;⁵⁻⁸ in the study of inhomogeneous fluids it is the starting point of most density functional theories;^{9,10} while the study of its collective dynamics is of outmost importance in understanding hydrodynamic long time tail correlations,^{11,12} the glass transition,¹³ or granular phenomena.¹

The interest of hard spheres as a fundamental theoretical abstraction was further revitalized in the 1980's with the discovery of colloidal hard spheres: the experimental realization of close to hard sphere models made from harshly repulsive spherical colloids.¹⁴ This allowed for a micrometer scale test of atomic scale problems, and a fruitful and long-lasting convergence of apparently distant scientific communities.¹

The similarity between hard spheres and their colloidal analogs has been confirmed for the freezing transition, the equation of state,^{15,16} and the spatial correlations.^{13,17} But the good agreement between experimental and in silico twins appears to breakdown when one looks at interfacial properties.¹ Measurement of the

crystal-melt interfacial stiffness coefficients of colloidal hard spheres show far less good agreement with computer simulations results for hard spheres.¹⁸⁻²¹ Intriguingly, experiments performed with colloids of finite buoyant mass,^{18,19} exhibit considerably more discrepancies than those performed with vanishing buoyant mass.^{20,21}

These differences immediately beg the question, as to whether gravity could possibly play any role in the experimentally measured stiffness coefficients.²² However, sedimentation profiles analysed in the light of the osmotic equation highlight the structural similarity of colloidal hard spheres with true hard spheres, suggesting no significant role of gravity in establishing static equilibrium properties.^{15,16,23} Further studies of the freezing transition in computer simulations emphasized the role of gravity and crystallization rate in selecting different crystal polymorphs, but established that slow crystallization rates and small initial volume fractions favor the growth of the expected equilibrium face centered cubic phase.²⁴⁻²⁷ Unfortunately, none of these studies addressed the calculation of the actual interfacial stiffness coefficients, so the reason for the discrepancy remains unsolved.

Here we perform computer simulations of crystal-melt interfaces under gravity and measure the stiffness coefficients from the spectrum of capillary wave fluctuations. Our results show that the stiffness picks up an explicit gravity dependence that is given by:²²

$$\tilde{\gamma} = \tilde{\gamma}_0 \left(1 + \frac{\xi^2}{\xi_{\parallel}^2} \right) \quad (1)$$

where $\tilde{\gamma}_0$ is the stiffness coefficient in the absence of gravity, ξ^2 is a measure of the interfacial width and ξ_{\parallel} is the capillary length. For atomic fluids, the ratio of ξ/ξ_{\parallel} is completely negligible, but for colloidal hard spheres, with large diameters and tunable buoyant mass, this ratio can

^{a)}Electronic mail: lmac@quim.ucm.es

^{b)}Electronic mail: eva.noya@iqf.csic.es

become significant and amenable to experimental measurement. Agreement of the computer simulation results with the above equation lends support to an interfacial displacement model which predicts quite generally an explicit dependence of stiffness coefficients with external fields.^{22,28-30}

II. RESULTS

A. Structure of the sedimented hard colloids

Sedimentation profiles obtained for pseudo-HS,³¹ using molecular dynamics simulations are displayed in Fig.1 for reduced gravity $\tilde{G} = m\sigma G/k_B T$ in the range from 0.25 to 2.0, with m , the buoyant mass, σ the hard sphere diameter, G the acceleration due to gravity and $k_B T$ the thermal energy. For large values of the vertical direction, z , the number density profiles, $\rho(z)$, shown in green, appear smooth, as in a fluid phase. Owing to the effect of gravity, the topmost layers build up a hydrostatic pressure, and compress the layers below, leading to a strongly stratified density profile akin to a crystal phase.

To check this, we have calculated the pressure components of the Irving-Kirkwood (IK) pressure tensor³², as well as the perpendicular pressure component as obtained from the Method of Planes (MOP). The results for the parallel component of the IK tensor are shown in blue, while those of the perpendicular component from the method of planes is shown in orange (both IK and MOP agree exactly within the scale of the figure). Similar to the density profile, the pressure tensor components gradually increase as z decreases. For the fluid phase, both parallel and perpendicular components agree exactly. In the crystal phase, the perpendicular component increases smoothly, as expected for the hydrostatic pressure, but a close up shows step-wise increases within the crystal phase. On the contrary, in the crystal phase the parallel component exhibits strong oscillations that are perfectly in phase with the density profile. For all values of \tilde{G} studied, it is confirmed that the onset of crystallization occurs when the pressure attains a value close to the freezing transition of $\beta p = 11.65$.

A quite accurate quasi-thermodynamic description of the sedimentation profile in the fluid phase may be achieved purely from knowledge of the equation of state of hard spheres. Indeed, the condition of thermodynamic equilibrium requires the system to exhibit equal chemical potential through-out the full system, despite the inhomogeneity of the density profile and the resulting pressure components. Whence, at some reference height z_0 , of chosen reference density, $\rho(z_0) = \rho_l$ the chemical potential is:

$$\mu_0 = \mu(\rho(z_0)) + mgz_0 \quad (2)$$

By the same token, at some other arbitrary position, z , the chemical potential is:

$$\mu_0 = \mu(\rho(z)) + mgz \quad (3)$$

Since the heights differ, the density needs to change in order for the global chemical potential to remain constant. As a result, the system develops a non-homogeneous sedimentation profile, dictated by the equation:

$$\mu(\rho(z)) - \mu(\rho_0) = mg(z - z_0) \quad (4)$$

Using the Carnahan-Starling equation of state, this yields right away:

$$\frac{3 - \eta}{(1 - \eta)^3} - \frac{3 - \eta_0}{(1 - \eta_0)^3} + \ln \frac{\eta}{\eta_0} = \beta mg(z - z_0) \quad (5)$$

The above result is a generalized hydrostatic equation for hard spheres which provides corrections to the barometric law. This local thermodynamic approximation works very well for all of the fluid phase, as indicated by the circles in Fig.1, which match almost exactly the sedimentation profile up to the onset of oscillatory behavior close to freezing, as already noticed long ago²³. This justifies the use of a local thermodynamic approach to obtain the equation of state from experimental sedimentation profiles^{15,16,33}. Moreover, the sedimentation profiles obtained from Eq.5 can be plugged into the Carnahan-Starling equation of state, and lead also to excellent predictions of the hydrostatic pressure, as illustrated by squares in Fig.1. Care should be taken when approaching the density of freezing, however. In this regime, the profiles become dictated by packing correlations of the order of the hard-sphere diameter, and require a weighted density approach to be described accurately^{9,10,23,34,35}.

An interesting observation from the pressure profiles of Fig.1 is the gradual loss of consistency between parallel and perpendicular components of the pressure tensor. Indeed, from the figure it becomes apparent that the parallel pressure cannot catch up with the gradual build-up of hydrostatic pressure. This can be appreciated by observing the slope of the lower envelope of the parallel pressure component, which is lower than that observed for the perpendicular component. This discrepancy shows the build-up of stress in the crystal phase, a result of the practical simulation setup. The perpendicular dimensions of the unit cell can accommodate the gradual build up of the simulation cell. However, the lateral dimensions of the simulation cell are fixed to the value corresponding to the equilibrium crystal at the freezing transition. Eventually, this mismatch leads, at the large pressure of $\tilde{G} = 2$, to a distortion of the crystal structure. This is already evidenced in the density profiles, where the amplitude of the density waves decrease significantly within the crystal center, and become much more rounded than for lower \tilde{G} . In the pressure tensor, this disruption is revealed by the inability of the lateral pressure oscillations to attain values greater than the perpendicular hydrostatic pressure.

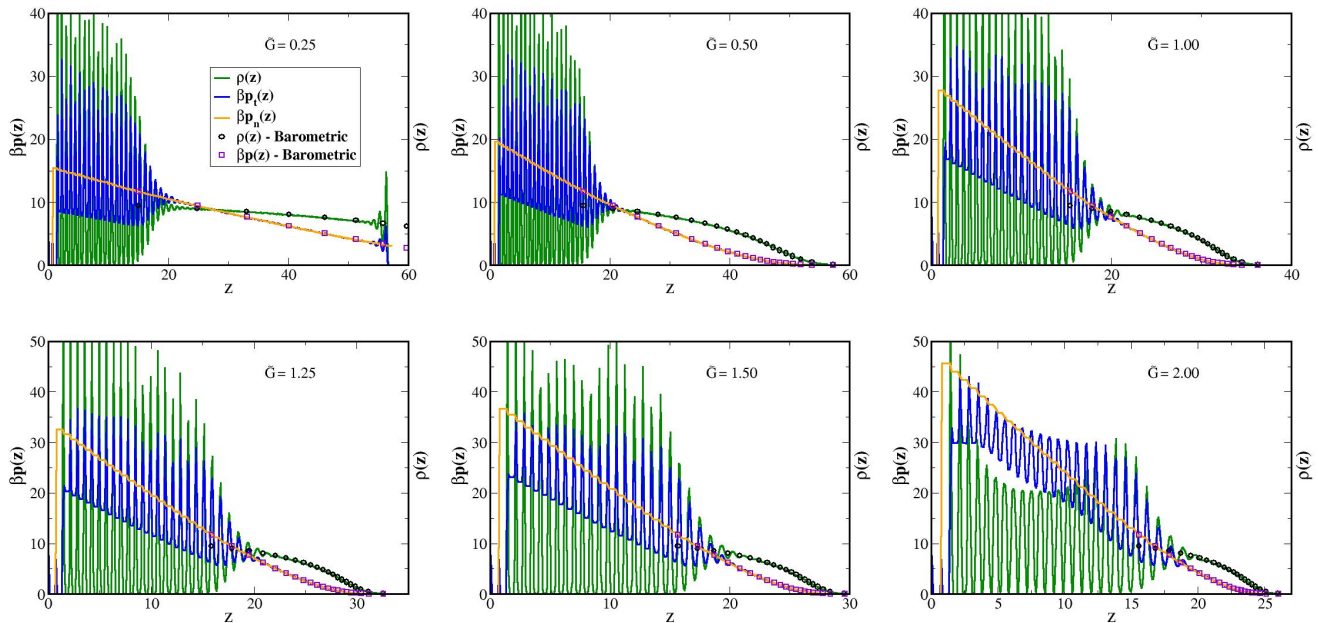


FIG. 1. Pressure and density profiles. The black and orange lines are the zz component of the pressure tensor by IK and MOP methods, which overlap one on top of the other. The red and blue are xx and yy components, which also overlap. Oscillations about the zz component suggest equilibrium. The system always crystallizes very close to the intersection of $p_{zz}(z)$ with the equilibrium coexistence pressure, as displayed by the dashed black line in the figures for $\beta p \sigma^3 = 11.65$, the estimated coexistence pressure of PHS.

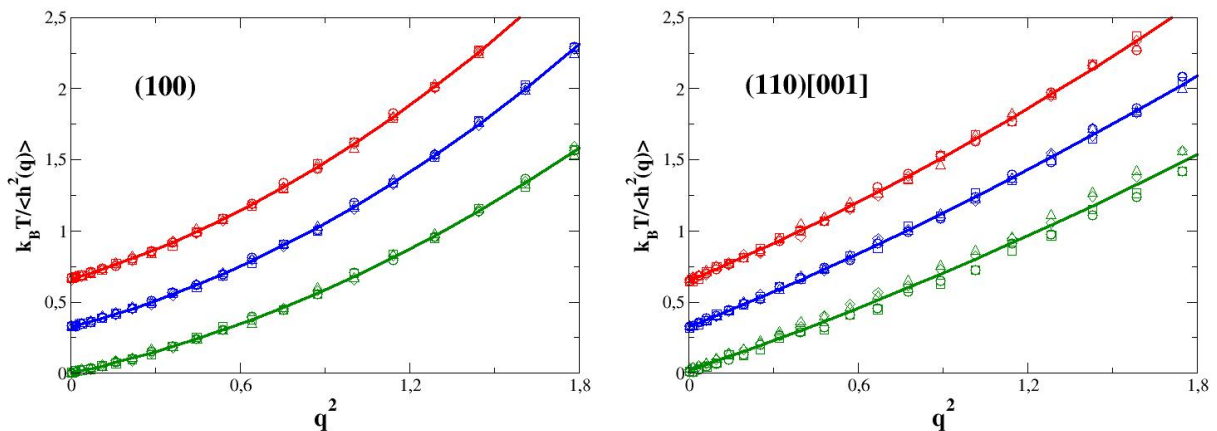


FIG. 2. Capillary wave spectrum for interfaces under gravity. Results are shown for surface fluctuations on the (100) interface (left) and the (110) interface along the [001] direction (right), with $\tilde{G} = 0$ (green), $\tilde{G} = 0.75$ (blue) and $\tilde{G} = 1.50$ (red). The symbols are average simulation results from four independent runs. The lines are fits to the 20 first wave-vectors to Eq.6. For ease of view, the results for $\tilde{G} = 0.75$ and $\tilde{G} = 1.5$ are shifted by 0.25 and 0.50 along the y axis, respectively.

B. Capillary fluctuations and interfacial stiffness

The above results show that for the relatively large gravity field of our simulations, the hydrostatic pressure created by the fluid phase is sufficient to drive the bottom part of the system into the crystal state. Accordingly,

the systems exhibit a fluid-crystal interface subject to gravity.

A convenient means of probing the interfacial properties is by studying the capillary wave spectrum. This is a measure of the mean squared amplitudes of interfacial fluctuations along directions parallel to an interface subject to a binding potential $g(h)$. In a quadratic or-

der approximation, the expression for the mean squared amplitude of the surface Fourier modes, $\langle h_q^2 \rangle$, is given by:³⁶⁻³⁹

$$\frac{k_B T}{A \langle h_q^2 \rangle} = g'' + \tilde{\gamma} q^2 + \kappa q^4 \quad (6)$$

where g'' is the second derivative of the binding potential, $\tilde{\gamma}$ is the interfacial stiffness coefficient of the fluid-crystal interface and κ , the bending rigidity, is added here in order to describe the expected wave-vector dependence of the spectrum in the large q regime.⁴⁰⁻⁴²

In our system, the free energy of rising the interface up to a height h against gravity is given by $g(h) = \frac{1}{2} m \Delta \rho G h^2$, where $\Delta \rho$ is the number density difference between the crystal and fluid phase. Whence, in the classical theory, all of the effect of the external field on the interface is to damp the spectrum of fluctuations in the limit of zero wave-vector by a term $g'' = m \Delta \rho G$.

The expectations from the classical capillary wave theory may be conveniently tested using computer simulations^{41,43-48}. For this purpose, we simulate large systems of HS using Monte Carlo simulations. In our system, we first identify solid-like atoms using the \bar{q}_6 parameter,⁴⁹ and then identify the interfacial height along the direction of fluctuations, $h(x)$ from the outermost atoms of the largest solid cluster (c.f. Methods). The resulting interfacial heights are Fourier transformed, squared and thermally averaged as a post-processing stage.

The plots shown in Fig.2 exhibit very good agreement with the simulated capillary wave-spectrum for a broad range of wave-vectors. Of course, this just shows that the spectrum of fluctuations can be accurately modeled with a second order polynomial in q^2 . To check the accuracy of the classical theory of capillary waves, we need to show that the parameters retrieved from the fit also match the classical expectation, i.e., that $g'' = m \Delta \rho \tilde{G}$, $\tilde{\gamma} = \tilde{\gamma}_0$ and $\kappa = \kappa_0$, with the $_0$ subscripts denoting the corresponding values in the absence of gravity.

The coefficients obtained from fits to Eq.6 as a function of \tilde{G} are illustrated in Fig.3. The results for g'' are found to obey very accurately the classical expectation. Using the bulk coexistence densities at the freezing transition,⁵⁰ we obtain $\Delta \rho \sigma^3 = 1.0369 - 0.9375 = 0.0994$, which used in $g'' = m \Delta \rho G$ provides an excellent match to the simulation data (c.f. straight line in Fig.3-a), except for an outlier at $\tilde{G} = 2$ from the (100) plane.

The situation is different for the next to leading order coefficient, however. Indeed, the stiffness coefficients retrieved from Eq.6 do not remain constant, as predicted by the classical capillary wave theory, but pick up a clear linear gravity dependence, as illustrated by a least square fit to the data (dashed line in Fig.3-b).

Such a linear dependence of the stiffness coefficient for an interface under gravity was conjectured to exist some time ago²⁸, and was shown to be obeyed for hard colloids in two dimensions²². In fact, this dependence is a particular case of a more general result for

the dependence of stiffness coefficients under arbitrary external fields^{29,30,52,53}. This non-classical phenomenology results from an interface displacement model which assumes the density of a corrugated interface, $\rho(\mathbf{r})$ is a function of the perpendicular distance away from the interface location.³⁰ This simplified ansatz describes non-local effects of interfacial fluctuations, an issue which has been studied in great detail by Parry and collaborators.⁵⁴ Using this approximation for the density profile, it may be shown that the stiffness coefficient under an external field becomes^{28,30}:

$$\tilde{\gamma} = \tilde{\gamma}_0 + g'' \xi^2 \quad (7)$$

where ξ is a bulk correlation length on the order of the interfacial width.

The formal proof of Eq.7 is lengthy^{22,55}, but a simple heuristic argument readily leads to the same result²². The rationale here is that the surface fluctuations of a weakly bound interface are correlated over long distances, as dictated by the parallel correlation length, $\xi_{\parallel}^2 = \tilde{\gamma}/g''$.^{37,38,56} For simple atomic fluids under usual gravity forces, the correlation length can become very large, exceeding in orders of magnitude any relevant atomic length-scale. Now, consider the opposite case of infinitely strong fields, where $g'' \rightarrow \infty$. In this limit, the capillary wave result under an assumed constant surface tension $\tilde{\gamma} = \tilde{\gamma}_0$ would predict that the parallel correlation length vanishes altogether, $\xi_{\parallel}^2 \rightarrow 0$. In practice, one expects that ξ_{\parallel} must be bound from below by the bulk correlation length of the fluid, ξ , until breakdown of the linear response regime. Assuming $\xi_{\parallel}^2 = \tilde{\gamma}/g''$ is generally valid for all fields, with $\tilde{\gamma}$ now allowed to depend on the external field, one finds that Eq.7 smoothly interpolates between the accepted result of capillary wave theory, $\tilde{\gamma}_0/g''$ when g'' is very small, and the lower bound, ξ^2 , expected for strong fields of similar order of magnitude than the prevailing interatomic forces in the fluid.

For the particular case of colloids under gravity, Eq.7 readily yields $\tilde{\gamma}(\tilde{G}) = \tilde{\gamma}_0 + m \Delta \rho \tilde{G} \xi^2$, which indeed leads to the linear dependence of $\tilde{\gamma}$ on \tilde{G} anticipated in Eq.1 and observed in Fig.3-b. Restricting the fit to data for $\tilde{G} < 2$, we find (c.f. full line in Fig.3-b):

$$\beta \tilde{\gamma}_{(100)} \sigma^2 = 0.420 \pm 0.008 + (0.12 \pm 0.01) \tilde{G} \quad (8)$$

$$\beta \tilde{\gamma}_{(110)} \sigma^2 = 0.689 \pm 0.015 + (0.10 \pm 0.02) \tilde{G} \quad (9)$$

From the slope of the fits, and the simulation results for $\Delta \rho \sigma^3 = 0.0994$ for the density gap at the freezing transition, this gives correlation lengths of about one molecular diameter, which appears as a reasonable value for a sharp interface in a first order phase transition (results give $\xi = 1.1\sigma$ and $\xi = 1.0\sigma$ for the (100) and (110) planes, respectively).

Figure 3-c displays the second order coefficient of the capillary wave expansion in powers of q^2 , often known as

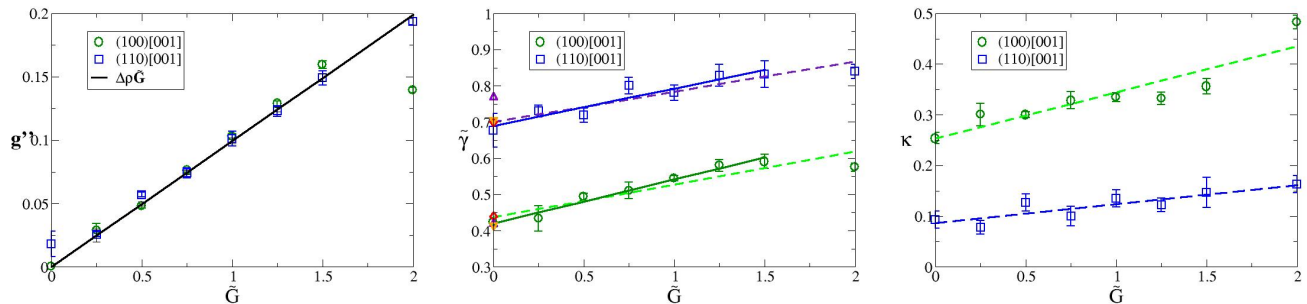


FIG. 3. Coefficients of the spectrum of fluctuations as obtained from simulation. Results for the (100)[001] direction are shown as circles, while those for the (110)[001] direction are shown as squares. For g'' , the line corresponds to the prediction $g'' = \Delta\rho\tilde{G}$ from capillary wave theory with no fitting parameters. For the other figures, lines are linear fits to the data. The middle panel also shows stiffness coefficients in zero gravity obtained from Ref.⁴⁵ (red diamonds), Ref.⁴⁷ (violet triangles up) and Ref.⁵¹ (orange triangles down).

the bending rigidity. The results suggest a linear dependence on gravity for this coefficient too, as indicated by the dashed lines obtained from linear regression. However, there is currently no theoretical account of an external field dependencies on κ , so it is difficult to discuss this further. It suffices to tell that, in the classical approach, all coefficients beyond g'' are assumed constants corresponding to the case of vanishing external field.

III. DISCUSSION

Synthetic hard sphere like colloids have been used for a long time as toy models of simple atomic fluids. These model systems exhibit an equation of state and freezing transition at conditions very similar to those found in computer simulations. However, reconciling experimental studies for the stiffness coefficients with results from computer simulations has proven far more difficult²². In experiments by Ramsteiner et al.,¹⁹ solutions of heavy hard sphere colloids with a significant buoyant mass produced stiffness coefficients close to twice larger than those found in computer simulations. On the contrary, experiments by van Loenen et al.,²¹ with solvent density matching that of the colloid, produced stiffness coefficients in far better agreement (Table Ref.III). Admittedly, the experiments are difficult, and the colloidal preparation varies from laboratory to laboratory,^{19,21} but the large difference observed for colloids mainly differing in the buoyant mass makes gravity a serious suspect for the discrepancy.

Van Loenen et al. noticed that the buoyant mass of the colloids in the experiment by Remsteiner et al. lead to very small gravitational length $\ell = k_B T/mg$ of ca. 0.14σ , and suggested the problem must have been related to the thickness of the fluid film atop the crystals. To understand the rationale, notice that the amount of liquid phase that can coexist above the crystal is limited by the imposed hydrostatic pressure. Any amount of matter withstanding sufficiently large pressure will freeze, so

that the thickness of the fluid phase above the crystal is not an independent variable; it depends on the imposed gravity. In our work, the smallest gravitational length $\ell = \tilde{G}^{-1}\sigma$ is 0.5σ , which results in a liquid film of barely 10σ thickness. (c.f. Fig.1). For the Remsteiner et al. experiment, the thickness of the film must have therefore been far smaller. In fact, Eq.5 suggests that the fluid film atop their crystal samples could have been just 3σ thick. The obvious question then is whether such a thin fluid phase could have affected the structure and properties of the crystal/melt interface.

This is a natural concern, and it is quite likely that for such thin films, the confinement of the fluid phase might have been responsible for part of the discrepancy. But our results show that the problem is far more subtle and not quite directly related to the thickness of the liquid column above the crystal. Indeed, we find that, irrespective of the liquid thickness, and definitively, for liquid thicknesses far larger than the packing correlations propagated from the crystal into the liquid (c.f. Fig.1), the stiffness coefficients exhibit a clear gravity dependence (Fig.3-b). This result is in agreement with Eq.7, which has previously been found to be accurate for the prediction of colloids in two dimensions,²² and for adsorbed liquid films on an attractive substrate, where the stiffness then picks up a complicated film thickness dependence that results from the external field imposed by the substrate on the film.^{28,29,52,53}

Support for Eq.7 does not only come from the simulation results in this work. The experimental results of heavy colloids by Remsteiner et al. can be made to agree within error bars to the computer simulations. This is illustrated in the fourth column of Table III, where the experimental results are corrected by the gravity effect predicted from Eq.7. By this operation, the results for heavy colloids are brought in far better agreement with those for weightless colloids and with results from computer simulations. Interestingly, the good agreement can be obtained by assuming a bulk correlation length of one single colloidal diameter, $\xi = 1\sigma$, which is essentially the

Orientation	g''	$\tilde{\gamma}^{\text{exp}}$	$\gamma^{\text{exp}} - \xi^2 g''$	Source
(100)[001]	0.57 ± 0.1	1.3 ± 0.3	0.67 ± 0.4	Ref. ¹⁹
(100)[001]	0	0.47 ± 0.3	0.47 ± 0.3	Ref. ²¹
(100)[001]	0	0.42 ± 0.1	0.42 ± 0.1	This work
(110)[001]	0.37 ± 0.1	1.0 ± 0.2	0.63 ± 0.3	Ref. ¹⁹
(110)[001]	0	0.53 ± 0.5	0.53 ± 0.5	Ref. ²¹
(110)[001]	0	0.68 ± 0.1	0.68 ± 0.1	This work

TABLE I. Comparison of experimental stiffness coefficients for hard colloids under gravity with simulations in zero field. The second and third columns collect results from the capillary wave-spectrum under different effective gravity. The fourth column subtracts the gravity correction of Eq.7 to the results, showing how they are now brought to reasonable agreement among themselves and to computer simulations in zero gravity. The calculations assume $\xi = \sigma$ as suggested from fits to the simulation data for the stiffness coefficients in Fig. 3.

same result obtained from fits to the computer simulation results. This allows to reconcile the different experimental results among themselves and with computer simulations, and allows us to tick positively interfacial properties as yet one more example of how current synthetic hard sphere colloids are representative of the good old hard spheres that have proved essential in our understanding of condensed phase behavior.

Since the stiffness coefficients are closely related to surface tension, a word of caution is important here, before closing. Namely, the gravity dependence reported here and predicted by Eq.7 only affects stiffness coefficients or surface tensions when measured as the result of capillary wave undulations. i.e, if the area of the interface were to be increased without ever changing the height of the interface profile, as if stretching the system's lateral area, the surface tension would be insensitive to the external field. The correction term in Eq.7 is only relevant when the surface area increments occur against the imposed external field. Another important observation is that the corrections are of the order ξ^2 . This means that, for usual molecular fluids, where ξ is in the angstrom scale, the corrections are completely irrelevant. An exciting possibility is the testing of Eq.7 for colloidal suspensions close to a demixing critical point. According to the theory of critical phenomena, weightless fluids will exhibit the vanishing of the surface tension as $\gamma \propto (T - T_c)^\mu$, with μ a positive critical exponent. But according to Eq.7, the vanishing of the surface tension as measured in a capillary wave experiment will compete with an additional contribution of order $\xi^2 \Delta\rho$. Close to the critical point under strong gravity,⁵⁷ the divergence of ξ would be limited by the gravity field and attain a constant value, whereupon the measured stiffness would scale as $\Delta\rho \propto (T - T_c)^\beta$. In view of the 3-d critical exponents, with $\mu \approx 1.26$ and $\beta \approx 0.32$,³⁷ the result of Eq.7 suggests a much slower decay of $\tilde{\gamma}$ than expected in absence of gravity. It is unclear whether Eq.7 can remain accurate up to the critical point, but testing this prediction using tailored colloidal suspensions with different buoyant masses appears as an

exciting experimental avenue.

IV. METHODS

Simulations have been performed for both Hard Spheres (HS) and pseudo-Hard Spheres (p-HS) under gravity. The former are carried out with an in-house parallel Monte Carlo code (MC)⁵⁸. The latter are carried out using molecular dynamics simulations (MD).

For either HS or p-HS, the total energy felt by a hard colloid is given by its pair potential, $u(r)$, plus an additional potential energy term due to gravity, mGz , where m is the buoyant mass of the colloid, G is the acceleration due to gravity, and z is a cartesian coordinate in the direction parallel to the gravity field.

For the computer simulations we use $k_B T$ as unit of energy, the HS diameter σ as unit of distance and the buoyant mass as unit of mass. This means the gravity pull is given by the dimensionless parameter $\tilde{G} = \beta m G \sigma$, with $\beta = 1/k_B T$. In these units, the total energy felt by colloid i is:

$$U_i = \sum_{i \neq j} u(r_{ij}) + \tilde{G}z \quad (10)$$

A. Monte Carlo Simulations

The MC simulations were performed to describe the behavior of actual Hard Spheres with diameter σ :

$$u(r) = \begin{cases} \infty & r < \sigma \\ 0 & r \geq \sigma \end{cases} \quad (11)$$

In order to speed up simulations for the rather large systems considered, we implemented a parallel GPU Monte Carlo. The simulation box is divided using a checkerboard decomposition⁵⁹ into cubic cells whose sides are slightly larger than the interaction range (the size of the particles in this case), so that trial MC attempts for particles belonging to non-neighboring cells can be performed simultaneously. As in our previous work⁵⁸, our implementation used 27 GPU threads per each cell (each of these threads calculates the change of energy in the central or in the 26 surrounding cells), significantly improving computational efficiency.

Rigid walls are placed at the bottom and top of the simulation box, specifically along the direction of the applied gravitational field (z in our case). The two bottom face-centred-cubic particle layers are kept frozen to minimize wall effects. While periodic boundary conditions are applied in the three dimensions of space, the box side along z is chosen to be at least one checkerboard cell edge longer than the distance between the top and bottom rigid walls. By using this trick, periodic boundary conditions effectively apply only along the x and y axes without requiring modification of the MC code.

Each interface was simulated over 2 million MC cycles (where each cycle is defined as 20 MC particle move attempts per cell). Four independent simulations were performed for each case. In each simulation run, 10 000 configurations were saved for the analysis.

This new MC algorithm was compared with sedimentation profiles obtained for p-HS using Molecular Dynamics simulations for the small (100) system. The comparison in Fig.4 shows no detectable differences between the two methods for all the range of gravity fields studied.

B. Molecular Dynamics Simulations

To carry out MD simulations, we used the p-HS model of Ref.³¹. Here, the hard colloids are described in the spirit of the Weeks-Chander-Andersen potential (WCA). This is build from a parent attractive pair-potential that is truncated and shifted by its well depth for distances smaller than the minimum and set to zero otherwise⁷. At odds with the standard WCA potential, the usual 12-6 exponents are replaced by 50-49 exponents so as to enforce a very steep repulsive branch:

$$u(r) = \begin{cases} \epsilon \left[40 \left(\frac{r_m}{r} \right)^{50} - 50 \left(\frac{r_m}{r} \right)^{49} \right] + \epsilon & r < \sigma \\ 0 & r \geq \sigma \end{cases} \quad (12)$$

where r_m is a factor 50/49 times larger than the effective hard sphere diameter σ .

MD simulations were carried out with LAMMPS,⁶⁰ using a time-step of $dt = 0.001$ reduced units and a Langevin thermostat. The gravitational pull was implemented using the `fix gravity` command and the reduced temperature was set to $k_B T / \epsilon = 1.5$ for optimal agreement with true HS.³¹

C. System setup

Simulations were performed for the hard colloids exposing either the (100) or the (110) facet of the face-centred-cubic (FCC) solid.

For the (100) case, we used two system sizes. Small systems were prepared as a stack of 5×5 FCC unit cells in the x and y directions, and up to 31 cells in the vertical direction, depending on \tilde{G} . Large systems were prepared as stacks of 60×5 unit cells, and between 15 to 31 unit cells in the vertical direction. In this way, the system is prepared so as to expose the (100) plane, while allowing for long wave-length capillary wave excitations along the x axis. Following the convention of Ref.⁴⁵, this setup is described as (100)[001], under the convention that (ijk) denotes the direction perpendicular to the exposed plane, while $[mnl]$ is the axis perpendicular to $[ijk]$ and the direction of wave propagation. In practice, this distinction is not relevant in this case, as the (100) plane of the FCC lattice is isotropic.

For the (110) plane, we considered only large systems, prepared as a stack of 90×5 unit cells oriented along the (110) direction and replicated up to 44 times in the vertical direction. For this plane, the crystal surface is anisotropic, and the settings are chosen such that the axis perpendicular to the plane and the direction of wave propagation is [001].

In either the small or large systems, the two bottom-most unit cells in the crystal stack were fixed in their equilibrium position, while the vertical dimensions of the box were enlarged so as to allow the system to melt spontaneously in the absence of gravity. The lateral dimensions were set for all values of \tilde{G} as to exactly match the corresponding equilibrium size of coexisting hard spheres, i.e., under an assumed crystal density of $\rho_c = 1.0369$.⁵⁰ For the p-HS simulations, the phase boundaries change slightly, and we assumed $\rho_c = 1.03994$, with a coexistence pressure at $\beta p = 11.65$.⁶¹

In this way, the initial configurations expose a perfectly mono-crystalline phase in the FCC state. In experiments, colloidal crystals are often multi-crystalline and exhibit stacking faults, but the approach to a perfect FCC phase is possible in principle by assembling the crystal from an initial state with low packing fraction and small sedimentation rate.²⁷ Notice that the (111) crystal orientation was avoided on purpose, as it is very difficult to prevent the formation of random hexagonal close packing at the interface²⁶.

D. Interface location

To locate the interface $h(x, y)$, we first characterize the local environment of each colloidal sphere using the neighbor-averaged \bar{q}_6 parameter⁴⁹. For this classification, two particles are considered first-neighbors if their separation distance is less than a cutoff of 1.35σ , which roughly corresponds to the first minimum in the radial distribution function of the bulk fluid. Using this cutoff, a threshold value of $\bar{q}_6^* = 0.327$ allows us to distinguish between liquid-like and solid-like colloids.

The solid phase is then identified as the largest solid cluster in the system (this serves to discard unconnected solid-like atoms occasionally forming within the bulk liquid), and selected for the location of the interfacial profile. To determine the interface position, the system is divided into rectangular prisms, centered at nodes on the $x-y$ plane. On each such prism, $h(x, y)$ is dictated as the average of the top most solid-like atoms inside the prism. The base of the prism and the number of atoms to average the interface location are chosen to be consistent with the crystal structure of the underlying bulk solid. The surface exposed face of the unit cell corresponds to the base of the prism; the number of atoms on the surface of that unit cell dictates the number of topmost atoms used to determine $h(x, y)$. In practice, since we only study the spectrum of fluctuations in the direction of the long x direction, we obtain a one dimensional interfacial profile

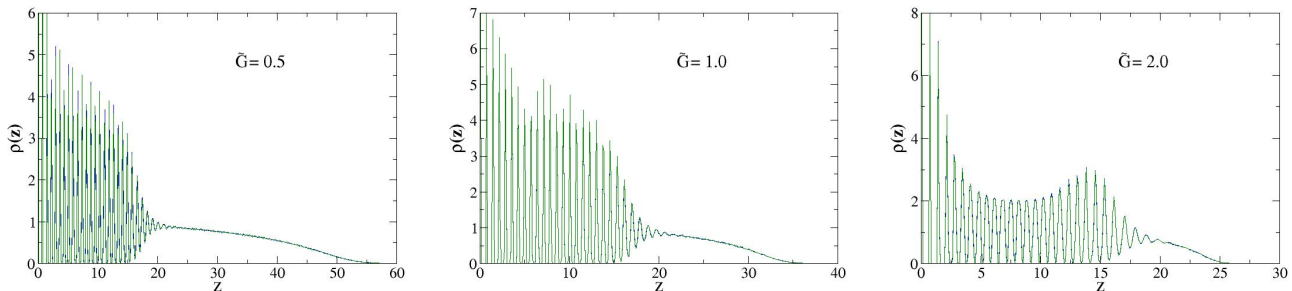


FIG. 4. Comparison of density profiles for HS and p-HS. Bluelines are density profiles from the pseudo-Hard Spheres, simulated by MD with LAMMPS. Green lines are results for HS, simulated with MC. The results do not show any difference in the scale of the plot.

$h(x)$ as the y average of $h(x, y)$. The number of nodes on the surface is dictated by the number of unit cells along the x and y directions of the simulation box. The instantaneous surface profile is then Fourier transformed and its thermal mean squared amplitude calculated. Averages are obtained from four independent runs, producing ten thousand configurations each.

V. ACKNOWLEDGEMENTS

We would like to thank Jürgen Horbach for helpful discussions. We would also like to acknowledge financial support from the Spanish Ministerio de Ciencia e Innovación and the Agencia Estatal de Investigación through grant PID2023-151751NB-I00 (MCIN/AEI/10.13039/501100011033).

- ¹C. P. Royall, P. Charbonneau, M. Dijkstra, J. Russo, F. Smallenburg, T. Speck, and C. Valeriani, “Colloidal hard spheres: Triumphs, challenges, and mysteries,” *Rev. Mod. Phys.* **96**, 045003 (2024).
- ²B. J. Alder and T. E. Wainwright, “Phase transition for a hard sphere system,” *J. Chem. Phys.* **27**, 1208 (1957).
- ³W. Wood and J. D. Jacobson, “Preliminary results from a recalculation of the Monte Carlo equation of state of hard spheres,” *J. Chem. Phys.* **27**, 1207 (1957).
- ⁴J. A. Barker and D. Henderson, “What is “liquid”? understanding the states of matter,” *Rev. Mod. Phys.* **48**, 587–671 (1976).
- ⁵J. A. Barker and D. Henderson, “Perturbation theory and equation of state for fluids. II. a successful theory of liquids,” *J. Chem. Phys.* **47**, 4714 (1967).
- ⁶G. A. Mansoori and F. B. Canfield, “Variational approach to the equilibrium thermodynamic properties of simple liquids. I,” *J. Chem. Phys.* **51**, 4958–4967 (1969).
- ⁷J. D. Weeks, D. Chandler, and H. C. Andersen, “Role of repulsive forces in determining the equilibrium structure of simple liquids,” *J. Chem. Phys.* **54**, 5237 (1971).
- ⁸A. Santos, S. B. Yuste, and M. López de Haro, “Structural and thermodynamic properties of hard-sphere fluids,” *J. Chem. Phys.* **153**, 120901 (2020).
- ⁹P. Tarazona, “Free-energy density functional for hard spheres,” *Phys. Rev. A* **31**, 2672–2679 (1985).
- ¹⁰Y. Rosenfeld, “Free-energy model for the inhomogeneous hard-sphere fluid mixture and density functional theory of freezing,” *Phys. Rev. Lett.* **63**, 980–983 (1989).

- ¹¹B. J. Alder and T. E. Wainwright, “Velocity autocorrelations for hard spheres,” *Phys. Rev. Lett.* **18**, 988–990 (1967).
- ¹²B. J. Alder and T. E. Wainwright, “Decay of the velocity autocorrelation function,” *Phys. Rev. A* **1**, 18–21 (1970).
- ¹³A. van Blaaderen and P. Wiltzius, “Real-space structure of colloidal hard-sphere glasses,” *Science* **270**, 1177–1179 (1995).
- ¹⁴P. Pusey and W. van Megen, “Phase behavior of concentrated solutions of nearly hard colloidal spheres,” *Nature* **320**, 340–342 (1986).
- ¹⁵S.-E. Phan, W. B. Russel, Z. Cheng, J. Zhu, P. M. Chaikin, J. H. Dunsmuir, and R. H. Ottewill, “Phase transition, equation of state, and limiting shear viscosities of hard sphere dispersions,” *Phys. Rev. E* **54**, 6633–6645 (1996).
- ¹⁶M. A. Rutgers, J. H. Dunsmuir, J.-Z. Xue, W. B. Russel, and P. M. Chaikin, “Measurement of the hard-sphere equation of state using screened charged polystyrene colloids,” *Phys. Rev. B* **53**, 5043–5046 (1996).
- ¹⁷A. Moussaïd and P. N. Pusey, “Multiple scattering suppression in static light scattering by cross-correlation spectroscopy,” *Phys. Rev. E* **60**, 5670–5676 (1999).
- ¹⁸J. Hernández-Guzmán and E. R. Weeks, “The equilibrium intrinsic crystal-liquid interface of colloids,” *Proc. Natl. Acad. Sci. U.S.A.* **106**, 15198–15202 (2009).
- ¹⁹I. B. Ramsteiner, D. A. Weitz, and F. Spaepen, “Stiffness of the crystal-liquid interface in a hard-sphere colloidal system measured from capillary fluctuations,” *Phys. Rev. E* **82**, 041603 (2010).
- ²⁰V. D. Nguyen, Z. Hu, and P. Schall, “Single crystal growth and anisotropic crystal-fluid interfacial free energy in soft colloidal systems,” *Phys. Rev. E* **84**, 011607 (2011).
- ²¹S. Z. van Loenen, T. E. Kodger, E. A. Padston, S. Nawar, P. Schall, and F. Spaepen, “Measurement of the stiffness of hard-sphere colloidal crystal-liquid interfaces,” *Phys. Rev. Mater.* **3**, 085605 (2019).
- ²²L. G. MacDowell, “Surface tension of bulky colloids, capillarity under gravity, and the microscopic origin of the kardar-parisizhang equation,” *Phys. Rev. E* **108**, L022801 (2023).
- ²³T. Biben, J. Hansen, and J. Barrat, “Density profiles of concentrated colloidal suspensions in sedimentation equilibrium,” *J. Chem. Phys.* **98**, 7330–7344 (1993).
- ²⁴J. Zhu, M. Li, R. Rogers, W. Meyer, R. H. Ottewill, STS-73 Space Shuttle Crew, W. B. Russel, and P. M. Chaikin, “Crystallization of hard-sphere colloids in microgravity,” *Nature* **387**, 883–885 (1997).
- ²⁵J. P. Hoogenboom, D. Derks, P. Vergeer, and A. van Blaaderen, “Stacking faults in colloidal crystals grown by sedimentation,” *J. Chem. Phys.* **117**, 11320–11328 (2002).
- ²⁶T. Dasgupta, J. R. Edison, and M. Dijkstra, “Growth of defect-free colloidal hard-sphere crystals using colloidal epitaxy,” *J. Chem. Phys.* **146**, 074903 (2017).

- ²⁷M. Marechal, M. Hermes, and M. Dijkstra, “Stacking in sediments of colloidal hard spheres,” *J. Chem. Phys.* **135**, 034510 (2011).
- ²⁸L. G. MacDowell, J. Benet, and N. A. Katcho, “Capillary fluctuations and film-height-dependent surface tension of an adsorbed liquid film,” *Phys. Rev. Lett.* **111**, 047802 (2013).
- ²⁹L. G. MacDowell, J. Benet, N. A. Katcho, and J. M. Palanco, “Disjoining pressure and the film-height-dependent surface tension of thin liquid films: New insight from capillary wave fluctuations,” *Adv. Colloid Interface Sci.* **206**, 150–171 (2014).
- ³⁰L. G. MacDowell, “Capillary wave theory of adsorbed liquid films and the structure of the liquid-vapor interface,” *Phys. Rev. E* **96**, 022801 (2017).
- ³¹J. Jover, A. J. Haslam, A. Galindo, G. Jackson, and E. A. Müller, “Pseudo hard-sphere potential for use in continuous molecular-dynamics simulation of spherical and chain molecules,” *J. Chem. Phys.* **137**, 144505 (2012).
- ³²J. H. Irving and J. G. Kirkwood, “The statistical mechanical theory of transport processes. IV. the equations of hydrodynamics,” *J. Chem. Phys.* **18**, 817 (1950).
- ³³R. E. Beckham and M. A. Bevan, “Interfacial colloidal sedimentation equilibrium. i. intensity based confocal microscopy,” *J. Chem. Phys.* **127**, 164708 (2007).
- ³⁴T. Biben, R. Ohnesorge, and H. Löwen, “Crystallization in sedimentation profiles of hard spheres,” *Europhys. Lett* **28**, 665 (1994).
- ³⁵Y.-X. Yu and J. Wu, “Structures of hard-sphere fluids from a modified fundamental-measure theory,” *The Journal of Chemical Physics* **117**, 10156–10164 (2002).
- ³⁶F. P. Buff, R. A. Lovett, and F. H. Stillinger, “Interfacial density profile for fluids in the critical region,” *Phys. Rev. Lett.* **15**, 621–623 (1965).
- ³⁷J. Rowlinson and B. Widom, *Molecular Theory of Capillarity* (Clarendon, Oxford, 1982).
- ³⁸J. R. Henderson, “Statistical mechanical sum rules,” in *Fundamentals of Inhomogeneous Fluids*, edited by D. Henderson (Marcel Dekker, New York, 1992) Chap. 2, pp. 23–84.
- ³⁹D. Nelson, T. Piran, and S. Weinberg, *Statistical Mechanics of Membranes and Surfaces* (World Scientific, Singapore, 2004).
- ⁴⁰K. R. Mecke and S. Dietrich, “Effective hamiltonian for liquid-vapor interfaces,” *Phys. Rev. E* **59**, 6766–6784 (1999).
- ⁴¹P. Tarazona, R. Checa, and E. Chacon, “Critical analysis of the density functional theory prediction of enhanced capillary waves,” *Phys. Rev. Lett.* **99**, 196101 (2007).
- ⁴²F. Höfling and S. Dietrich, “Enhanced wavelength-dependent surface tension of liquid-vapour interfaces,” *Europhys. Lett* **109**, 46002 (2015).
- ⁴³I. Benjamin, “Theoretical study of the water/1,2-dichloroethane interface: Structure, dynamics, and conformational equilibria at the liquid-liquid interface,” *J. Chem. Phys.* **97**, 1432–1445 (1992).
- ⁴⁴M. Müller and L. G. MacDowell, “Interface and surface properties of polymer solutions: Monte Carlo simulations and self-consistent field theory,” *Macromolecules* **33**, 3902–3923 (2000).
- ⁴⁵R. L. Davidchack, J. R. Morris, and B. B. Laird, “The anisotropic hard-sphere crystal-melt interfacial free energy from fluctuations,” *J. Chem. Phys.* **125**, 094710 (2006).
- ⁴⁶R. E. Rozas and J. Horbach, “Capillary wave analysis of rough solid-liquid interfaces in nickel,” *Europhys. Lett* **93**, 26006 (2011).
- ⁴⁷A. Härtel, M. Oettel, R. E. Rozas, S. U. Egelhaaf, J. Horbach, and H. Löwen, “Tension and stiffness of the hard sphere crystal-fluid interface,” *Phys. Rev. Lett.* **108**, 226101 (2012).
- ⁴⁸R. E. Rozas, L. G. MacDowell, P. G. Toledo, and J. Horbach, “Crystal growth of bcc titanium from the melt and interfacial properties: A molecular dynamics simulation study,” *J. Chem. Phys.* **154**, 184704 (2021).
- ⁴⁹W. Lechner and C. Dellago, “Accurate determination of crystal structures based on averaged local bond order parameters,” *J. Chem. Phys.* **129**, 114707 (2008).
- ⁵⁰E. G. Noya, C. Vega, and E. de Miguel, “Determination of the melting point of hard-spheres from direct coexistence methods,” *J. Chem. Phys.* **128**, 154507 (2008).
- ⁵¹J. Benet, L. G. MacDowell, and E. Sanz, “Computer simulation study of surface wave dynamics at the crystal-melt interface,” *J. Chem. Phys.* **141**, 034701 (2014).
- ⁵²J. Benet, J. G. Palanco, E. Sanz, and L. G. MacDowell, “Disjoining pressure, healing distance, and film height dependent surface tension of thin wetting films,” *J. Phys. Chem. C* **118**, 22079–22089 (2014).
- ⁵³L. G. MacDowell, P. Llombart, J. Benet, J. G. Palanco, and A. Guerrero-Martinez, “Nanocapillarity and liquid bridge-mediated force between colloidal nanoparticles,” *ACS Omega* **3**, 112–123 (2018).
- ⁵⁴N. R. Bernardino, A. O. Parry, C. Rascón, and J. M. Romero-Enrique, “Derivation of a nonlocal interfacial model for 3d wetting in an external field,” *J. Phys.: Condens. Matter* **21**, 465105 (2009).
- ⁵⁵L. G. MacDowell, “Surface van der waals forces in a nutshell,” *J. Chem. Phys.* **150**, 081101 (2019).
- ⁵⁶P. G. de Gennes, F. Brochard-Wyart, and D. Quéré, *Capillarity and Wetting Phenomena* (Springer, New York, 2004) pp. 1–292.
- ⁵⁷M. R. Moldover, J. V. Sengers, R. W. Gammon, and R. J. Hocken, “Gravity effects in fluids near the gas-liquid critical point,” *Rev. Mod. Phys.* **51**, 79–99 (1979).
- ⁵⁸E. G. Noya, “GPU parallel Monte Carlo code for patchy particles,” https://github.com/evanoya/MC_GPU (2026), 2021.
- ⁵⁹J. A. Anderson, E. Jankowski, T. L. Grubb, M. Engel, and S. C. Glotzer, “Massively parallel Monte Carlo for many-particle simulations on GPUs,” *J. Comput. Phys.* **254**, 27–38 (2013).
- ⁶⁰A. P. T. et al., “LAMMPS - a flexible simulation tool for particle-based materials modeling...” *Comp. Phys. Comm.* **271**, 108171 (2022).
- ⁶¹J. R. Espinosa, E. Sanz, C. Valeriani, and C. Vega, “On fluid-solid direct coexistence simulations: The pseudo-hard sphere model,” *J. Chem. Phys.* **139**, 144502 (2013).